

Spherical ansatz for parameter-space metrics

Bruce Allen

MPI for Gravitational Physics, Callinstrasse 38, Hannover, Germany

(Dated: October 31, 2021)

A fundamental quantity in signal analysis is the metric g_{ab} on parameter space, which quantifies the fractional “mismatch” m between two (time- or frequency-domain) waveforms. When searching for weak gravitational-wave or electromagnetic signals from sources with unknown parameters λ (masses, sky locations, frequencies, etc.) the metric can be used to create and/or characterize “template banks”. These are grids of points in parameter space; the metric is used to ensure that the points are correctly separated from one another. For small coordinate separations $d\lambda^a$ between two points in parameter space, the traditional ansatz for the mismatch is a quadratic form $m = g_{ab}d\lambda^a d\lambda^b$. This is a good approximation for small separations but at large separations it diverges, whereas the actual mismatch is bounded. Here we introduce and discuss a simple “spherical” ansatz for the mismatch $m = \sin^2(\sqrt{g_{ab}d\lambda^a d\lambda^b})$. This agrees with the metric ansatz for small separations, but we show that in simple cases it provides a better (and bounded) approximation for large separations, and argue that this is also true in the generic case. This ansatz should provide a more accurate approximation of the mismatch for semi-coherent searches, and may also be of use when creating grids for hierarchical searches that (in some stages) operate at relatively large mismatch.

I. MATCHED FILTERING AND THE OVERLAP BETWEEN TEMPLATES

More than two decades ago, when the first generation of interferometric gravitational wave (GW) detectors were still in the planning stages, a handful of pioneers investigated the techniques that would be needed to detect GW signals [1–10]. At that time there were three main challenges. First, the signals were weak in comparison with the noise from the detectors, so needed to be “teased out” of the data stream with optimal or near-optimal methods. Second, the parameters describing the signals (such as the object masses in a binary system, or the rotation frequency and spindown rate of a neutron star) were not known. This required repeated searches for signals with many different parameter combinations, creating a significant computational challenge. Lastly, even if the parameters were known precisely, for some sources the waveforms could only be calculated approximately. The errors could be estimated but not sharply quantified.

The solution to the first problem is to use “matched filtering” [3, 6–8, 11–16]. In the simplest case [17] the time-dependent output $S(t)$ of the detector is correlated with a template $T(t)$ to produce a statistic

$$\rho = (T, S). \quad (1.1)$$

If the template is normalized $(T, T) = 1$ then ρ is called the signal-to-noise ratio (SNR). This is reviewed in a signal-processing context in [18, 19] and in the GW context in [20] and [21].

The positive-definite inner product in Eq. (1.1) can be expressed in different ways. For example if the instrument noise is white (or the signal is confined to a narrow enough range of frequency that the noise is white in that

band) then the inner product is

$$(A, B) = \mathcal{N} \int A(t)B(t) dt, \quad (1.2)$$

where the integral extends over the support of the waveform or the duration of the data (whichever is shorter). The normalization constant \mathcal{N} is set by requiring that the expected value of (S, S) is unity where $S(t)$ is the detector output in the absence of any signals [22].

If the detector noise is colored [11] then the inner product is most simply expressed in the frequency domain as

$$(A, B) = \int_{-\infty}^{\infty} \frac{\tilde{A}^*(f)\tilde{B}(f)}{S(|f|)} df. \quad (1.3)$$

Here, the Fourier transform of a function of time $h(t)$ is denoted by $\tilde{h}(f)$, where f is frequency, and $S(f)$ is the (single-sided) noise power spectrum of the instrument.

For real instrument data sampled at a finite rate the integral in Eq. (1.2) may be replaced with a sum over samples and the integral in Eq. (1.3) may be replaced with a sum over Nyquist-sampled frequency bins [23].

The solution to the second problem is to construct the SNR ρ in Eq. (1.1) for many different templates T_{λ_i} , where λ are the parameters that describe the waveform and the integer i labels a finite set of distinct points which are being sampled from parameter space [3, 10, 11, 16, 24–33]. λ denotes the collection of coordinates in parameter space; the individual coordinates are denoted by λ^a where the index $a = 1, 2, \dots, N$ runs over the parameter-space coordinates.

For GWs from compact binary coalescence (CBC) λ includes the masses of the objects, sky location, orbital inclination, time of the merger, spins (if relevant) and so on. For continuous gravitational waves (CW) from a spinning neutron star λ includes the sky location, frequency and frequency derivative, and so on [34] [35–39].

The set of templates is called a template bank, and the art is in selecting their locations λ_i [16, 25–33, 38–65]. Since the signals themselves come from a continuous family and the template bank is discrete, real signals will not have parameters that exactly match any template in the bank. So one must ensure that there is at least one template “close enough” to the signal that it is not missed. At the same time, since ρ must be computed for each template, the number of templates should be no larger than needed. For the advanced LIGO and Virgo instruments, the CBC searches employ $O(10^5)$ templates; the CW searches employ orders of magnitude more.

To place the templates in parameter space, an important quantity is the overlap (also called a fitting function or match) between two templates

$$o(\lambda, \lambda') = (T_\lambda, T_{\lambda'}). \quad (1.4)$$

Because the templates are normalized, and the inner product is positive definite, the overlap lies in the closed interval $o \in [-1, 1]$ [66].

The overlap is also relevant to the third of the challenges described above because it may be used to quantify the loss in SNR arising from inaccuracies in the waveform models. However in this paper we assume that the waveform models are exact, and concentrate on the previous issue.

II. THE MISMATCH AND THE METRIC APPROXIMATION TO THE MISMATCH

Rather than using the overlap, it is more convenient to use a related quantity called the mismatch, but the literature contains several different definitions for this. Much of the work on CBC data analysis uses the mismatch $1 - o$ and much of the literature on CW signals uses $1 - o^2$. Here, we follow the latter convention, defining the mismatch as

$$m(\lambda, \lambda') = 1 - o^2(\lambda, \lambda'). \quad (2.1)$$

This mismatch lies in the interval $[0, 1]$ and is the fractional loss in the square of the expected SNR $\langle \rho \rangle^2$ that arises when a signal with parameters λ is detected using a template with parameters λ' . Sec. VIII gives results for another common definition, where the mismatch is the fractional loss of the expected SNR $\langle \rho \rangle$. In the Neyman–Pearson approach, m is the fractional loss in the maximum of the log likelihood ratio in the strong signal limit.

We note that a signal search algorithm may (either analytically or explicitly) minimize the mismatch with respect to some of the intrinsic or extrinsic parameters. In this case we assume that these parameters are not included in the vector λ and that the right-hand side (rhs) of the expression in Eq. (2.1) for m is minimized over those missing parameters [67] In hierarchical searches, the mismatch may also be averaged over data segments; we return to this in Sec. VII.

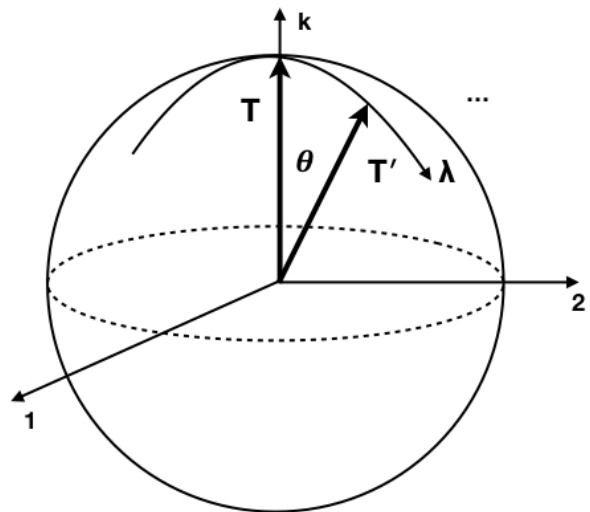


FIG. 1. The normalized templates $T = T(\lambda)$ and $T' = T(\lambda')$ may be thought of as unit vectors lying on the surface of a $(k - 1)$ -sphere, where the embedding dimension k is the number of discrete time-domain samples in the waveform (only three of these dimensions are shown here). A one-dimensional variation of the parameters λ traces out a path on the sphere, where the angular separation θ between the points is defined by $\cos \theta = (T, T')$.

It is helpful to think of the normalized templates $T = T_\lambda$ and $T' = T_{\lambda'}$ as unit-length vectors which lie on the surface of the unit sphere S^{k-1} as illustrated in Fig. 1. In the case where the data and template are discretely sampled, k is the number of samples in the template. In the continuous case k is infinite and the sphere is embedded in a Hilbert space [68].

We define the angle $\theta(\lambda, \lambda')$ between two normalized templates via

$$\cos \theta(\lambda, \lambda') = o(\lambda, \lambda') = (T, T') \quad (2.2)$$

so that the mismatch may be expressed as

$$m(\lambda, \lambda') = 1 - \cos^2 \theta = \sin^2 \theta. \quad (2.3)$$

Since the mismatch is extremal and vanishes at $\lambda = \lambda'$ it can be expanded in a Taylor series which (generically) begins at quadratic order.

This “metric approximation” to the mismatch has a geometrical interpretation which was introduced in [40] and elaborated in [14–16]. It is

$$m(\lambda, \lambda') = g_{ab} d\lambda^a d\lambda^b + O(q_{abc} d\lambda^a d\lambda^b d\lambda^c), \quad (2.4)$$

where $d\lambda = \lambda - \lambda'$, and we adopt the “Einstein summation convention” that repeated indices a, b, \dots, c are summed from 1 to N . The quantity g_{ab} is called the parameter-space metric [40]; for nearby templates, $g_{ab} d\lambda^a d\lambda^b$ measures the squared fractional deviation or squared dimensionless “interval” between the templates.

We note that there are other possible definitions of the metric, but this choice is normally adopted for the

template placement problem, because templates must be placed “independently of the data” based on the expected properties of the signals and detector noise. A good discussion of this and of other possible definitions of parameter-space metrics may be found in the Introduction and in Appendix A of Prix [69, 70].

III. SIMPLE ILLUSTRATIVE EXAMPLE

To make this concrete, we consider a simple CW example. The waveforms are described by a single (angular) frequency parameter $\lambda^1 = \omega$. In the time domain the normalized templates are

$$T_\omega(t) = \sqrt{\frac{1}{\tau}} \sin(\omega t) \quad \text{for } t \in [-\tau, \tau] \quad (3.1)$$

and vanish for $|t| > \tau$. In the cases of interest τ would be days to years, and ω would be tens to hundreds of cycles per second.

The overlap and mismatch between two templates may be easily computed, starting from Eq. (1.2) with $\mathcal{N} = 1$:

$$\begin{aligned} (T, T') &= \frac{1}{\tau} \int_{-\tau}^{\tau} \sin(\omega t) \sin(\omega' t) dt \\ &= \frac{\sin(\omega - \omega')\tau}{(\omega - \omega')\tau} - \frac{\sin(\omega + \omega')\tau}{(\omega + \omega')\tau}. \end{aligned} \quad (3.2)$$

For the cases of interest ω is large enough that there are many cycles in the interval $t \in [-\tau, \tau]$, and the fractional difference between ω and ω' is small. This means that the second term on the rhs of Eq. (3.2) is negligible, so the mismatch is given by the square of the sinc function

$$m = 1 - (T, T')^2 = 1 - \left[\frac{\sin \tau \Delta\omega}{\tau \Delta\omega} \right]^2, \quad (3.3)$$

where $\Delta\omega = \omega - \omega'$. This may be expanded as a Taylor series for small $\Delta\omega$, yielding $m = \frac{1}{3}\tau^2\Delta\omega^2 + O(\Delta\omega^4)$. Thus the metric is $g_{\omega\omega} = \tau^2/3$ and the metric approximation to the mismatch is

$$m = \frac{1}{3}\tau^2\Delta\omega^2. \quad (3.4)$$

IV. THE METRIC APPROXIMATION AND THE SPHERICAL APPROXIMATION

Shown in Fig. 2 (blue) is the actual mismatch m as a function of $\lambda - \lambda' = \Delta\omega$, as given by Eq. (3.3). Also shown (orange) is the metric approximation from Eq. (3.4). One can see that these agree well for small values of $\Delta\omega$, but that the metric approximation breaks down when $|\Delta\omega| \gtrsim 1/\tau$. One can also see that where they deviate, the quadratic approximation tends to *overestimate* the mismatch. This is well known to the experts [71] and frequently observed when the metric approximation is

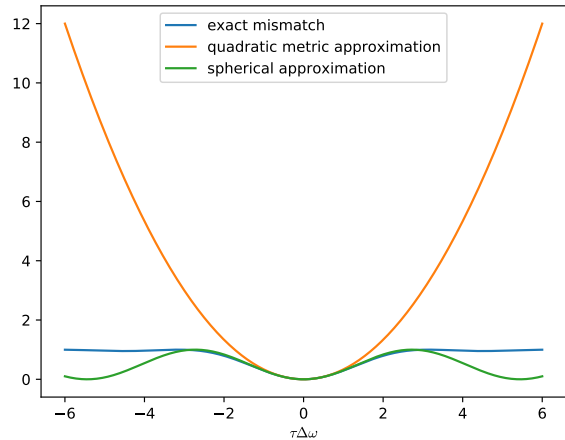


FIG. 2. The blue curve shows the mismatch m from Eq. (3.3) for long-duration sinusoidal signals of frequency ω and ω' , as a function of the frequency difference $\Delta\omega = \omega - \omega'$. The orange curve is the conventional metric approximation to the mismatch, given in Eq. (3.4). The green curve shows the spherical approximation to the mismatch, given in Eq. (4.3). While both approximations agree for small $|\Delta\omega|$, one can see that the spherical approximation is more accurate and has a larger domain of applicability. This is generically true because the spherical ansatz has one approximation fewer than the conventional metric ansatz.

compared to the true mismatch. Below we provide both the explanation and a simple solution.

It is helpful to visualize this on the sphere. Imagine that we have a path in parameter space, parameterized by the variable λ as shown in Fig. 1, which passes through the template T at parameter value λ , and T' at parameter value λ' . A generic parameterization is one for which the angle θ varies linearly with $\lambda - \lambda'$ for small values of θ [72].

For such a generic parameterization, the angular separation on the sphere is well approximated by

$$\theta = \sqrt{g_{ab} d\lambda^a d\lambda^b}. \quad (4.1)$$

This means that the mismatch can be written (in what we here call the “spherical approximation”) as

$$m = \sin^2 \theta = \sin^2 \sqrt{g_{ab} d\lambda^a d\lambda^b}. \quad (4.2)$$

The point of this short paper is that Eq. (4.2) is a better approximation to the generic mismatch than the more conventional approximation $m = g_{ab} d\lambda^a d\lambda^b$. While both of these approximations agree to lowest order in the parameter separation $d\lambda^a$, for the generic case the approximation given in Eq. (4.2) will be accurate for a larger range in $d\lambda^a$. It also has the advantage of always lying in the interval $[0, 1]$.

The simple example presented in Sec. III is a good demonstration of this. Fig. 2 shows how the behavior

of the conventional metric approximation (orange curve) deviates from the actual mismatch (blue curve) as the parameter mismatch $\Delta\omega$ increases. The spherical approximation (green curve) given by

$$m = \sin^2 \sqrt{g_{ab} d\lambda^a d\lambda^b} = \sin^2 \frac{\tau \Delta\omega}{\sqrt{3}} \quad (4.3)$$

is a much better fit to the actual mismatch. It deviates significantly from the actual mismatch only after the path on the sphere has exceeded a 90-degree separation between T and T' .

V. A SECOND EXAMPLE

The reader might ask if we have “tuned” our example in Sec. III. This is not so: the dependence upon the parameter (frequency) is quite typical. Here we present another typical case, where the signal model depends upon an offset phase parameter ϕ .

For this example, the normalized time domain templates are

$$T_\phi(t) = \sqrt{\frac{1}{\tau}} \sin(\omega t + \phi) \quad \text{for } t \in [-\tau, \tau], \quad (5.1)$$

and vanish for $|t| > \tau$. As in our previous example, we assume that the signal goes through many cycles in the observation interval, so that $\omega\tau \gg 1$ is large.

The overlap between templates is easily calculated from 1.2, giving

$$\begin{aligned} (T, T') &= (T_\phi, T_{\phi'}) \\ &= \frac{1}{\tau} \int_{-\tau}^{\tau} \sin(\omega t + \phi) \sin(\omega t + \phi') dt \\ &= \cos(\phi - \phi') - \frac{\sin 2\omega\tau}{2\omega\tau} \cos(\phi + \phi'). \end{aligned} \quad (5.2)$$

Since we are assuming that $\omega\tau \gg 1$, the second term on the rhs can be neglected, giving the mismatch

$$m = 1 - (T, T')^2 = \sin^2 \Delta\phi, \quad (5.3)$$

where $\Delta\phi = \phi - \phi'$.

In this case, the metric approximation to the mismatch yields the quadratic form $m = g_{ab} d\lambda^a d\lambda^b = (\Delta\phi)^2$. In contrast, the spherical approximation to the mismatch gives

$$m = \sin^2 \sqrt{g_{ab} \lambda^a d\lambda^b} = \sin^2 \Delta\phi. \quad (5.4)$$

So in our second example, the spherical approximation is exact!

VI. A THIRD EXAMPLE

In our final example, the signal parameter is a constant frequency derivative $\lambda^1 = \dot{\omega}$. The normalized time

domain templates are

$$T_{\dot{\omega}}(t) = \sqrt{\frac{1}{\tau}} \sin(\omega t + \dot{\omega} t^2 / 2) \quad \text{for } t \in [-\tau, \tau], \quad (6.1)$$

and vanish for $|t| > \tau$. We assume that (half of the) dimensionless phase accumulated during the observation time $\omega\tau + \dot{\omega}\tau^2/2$ is much larger than 2π .

The overlap between templates is

$$\begin{aligned} (T, T') &= (T_{\dot{\omega}}, T_{\dot{\omega}'}) \\ &= \frac{1}{\tau} \int_{-\tau}^{\tau} \sin(\omega t + \dot{\omega} t^2 / 2) \sin(\omega t + \dot{\omega}' t^2 / 2) dt \\ &= \frac{1}{2\tau} \int_{-\tau}^{\tau} \cos(|\Delta\dot{\omega}| t^2 / 2) dt \\ &= \sqrt{\frac{\pi}{|\Delta\dot{\omega}| \tau^2}} C\left(\sqrt{\frac{|\Delta\dot{\omega}| \tau^2}{\pi}}\right), \end{aligned} \quad (6.2)$$

where $C(z)$ is the Fresnel integral function, $\Delta\dot{\omega} = \dot{\omega} - \dot{\omega}'$, and we have dropped small terms from the rhs in the third line of Eq. (6.2).

The exact mismatch is given by

$$m(\dot{\omega}, \dot{\omega}') = 1 - \frac{\pi}{|\Delta\dot{\omega}| \tau^2} C^2\left(\sqrt{\frac{|\Delta\dot{\omega}| \tau^2}{\pi}}\right). \quad (6.3)$$

This is plotted in blue in Fig. 3. Since $C(z) = z - \frac{\pi^2}{40} z^5 + O(z^9)$ for small z , the normal metric approximation to the mismatch is $m = \tau^4 \Delta\dot{\omega}^2 / 20$. This is plotted in orange. Shown in green is the spherical approximation to the mismatch, $m = \sin^2(\tau^2 \Delta\dot{\omega} / \sqrt{20})$.

As in the previous examples, the spherical approximation is a better fit to the true mismatch.

VII. WHY DOES IT MATTER?

Why does this matter? After all, the metric approximation is only defined to quadratic order, and the mismatch can be expanded to higher order if needed. The point here is that there are really two approximations taking place. The first is in the Taylor approximation of the separation θ on the sphere, and the second is in the Taylor approximation of the sin function in the expression $\sin^2 \theta$ which relates the mismatch to θ . The conventional metric ansatz makes *both* of these approximations, whereas the spherical ansatz only uses the first of these approximations. So for generic behavior of the path in parameter space, the spherical ansatz will be more accurate than the metric ansatz. And since the spherical approximation just replaces $m = g_{ab} d\lambda^a d\lambda^b$ with $m = \sin^2 \sqrt{g_{ab} d\lambda^a d\lambda^b}$, this comes with no additional analytic or computational cost.

A more accurate approximation is useful because the metric is often used to construct grids in parameter space [25–33, 38, 46, 47, 49, 50, 73–77]. In situations where a search is not compute-power limited, these grids typically

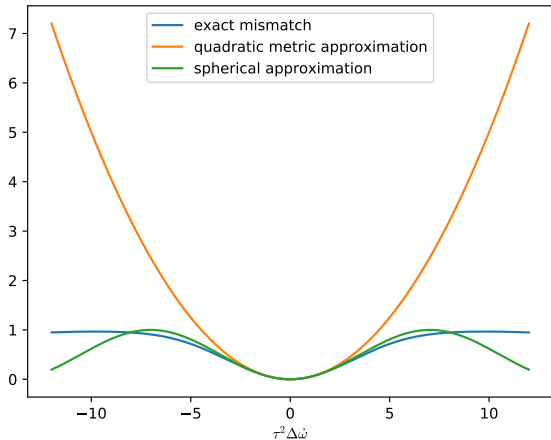


FIG. 3. The blue curve shows the true mismatch m from Eq. (6.3) for long-duration sinusoidal signals with constant frequency derivative, as a function of the frequency derivative difference $\Delta\omega = \omega - \omega'$. The orange curve is the conventional metric approximation to the mismatch, and the green curve shows the spherical approximation to the mismatch. As in the other examples, the spherical approximation is more accurate.

have a low mismatch. For example in CBC searches the traditional SNR mismatch is chosen at 3%, corresponding to an SNR^2 mismatch of 6%. For such small mismatches, the fact that $\sin\theta \approx \theta$ for small θ means that there is no significant difference between the metric and spherical approximations. However this may not be so for searches which are compute-power limited, for example in the search for CWs or the search for gamma-ray pulsars.

These computationally-limited searches often employ multiple hierarchical stages, which mix semi-coherent and coherent stages, each employing its own metric for template placement [28, 39, 46, 69, 70, 78–90]. Those hierarchical stages sometimes operate at substantial mismatches in the range $m \in [0.5, 0.7]$, and here, the spherical approximation is an improvement on the conventional quadratic approximation.

We can illustrate this using the example from Sec. III. Suppose we set up a one-dimensional grid in frequency ω , with a spacing $\Delta\omega$ picked to give a desired mismatch m . The metric approximation in Eq. (3.4) gives a parameter-space grid spacing

$$\Delta\omega = \frac{\sqrt{3}}{\tau} \sqrt{m}, \quad (7.1)$$

whereas the spherical approximation gives a grid spacing

$$\Delta\omega = \frac{\sqrt{3}}{\tau} \arcsin \sqrt{m}. \quad (7.2)$$

Effectively, the spherical approximation amounts to replacing the conventional metric mismatch m with

Mismatch m	Metric approximation grid spacing $\Delta\omega$	Spherical approximation grid spacing $\Delta\omega$
0.01	$0.173/\tau$	$0.173/\tau$
0.02	$0.245/\tau$	$0.246/\tau$
0.05	$0.387/\tau$	$0.391/\tau$
0.1	$0.548/\tau$	$0.557/\tau$
0.2	$0.775/\tau$	$0.803/\tau$
0.5	$1.225/\tau$	$1.360/\tau$
0.7	$1.449/\tau$	$1.717/\tau$
0.9	$1.643/\tau$	$2.163/\tau$

TABLE I. One-dimensional grid spacings $\Delta\omega$ for the simple example in Sec. III, comparing conventional versus spherical approximation to the metric. These agree for small mismatch, but diverge for mismatches approaching unity. Such large mismatches may be used in (multi-stage hierarchical) searches which are computing-power limited.

$(\arcsin \sqrt{m})^2$. The effect of this on the grid spacings is shown in Table I.

The spherical approximation might also provide a significant improvement for semi-coherent searches, when compared with the normal quadratic metric approximation. Semi-coherent methods are employed for computationally-limited electromagnetic and GW searches, and consist of breaking a long data stream into M shorter “computationally-feasible” segments, each of which is searched using traditional matched-filter methods. The resulting “coherent” statistics (typically SNR values) are then summed to produce the semi-coherent statistic, as first proposed in [35, 36]. To set up a template grid one computes a semi-coherent metric \bar{g}_{ab} to predict the fractional loss of the semi-coherent statistic. Until now \bar{g}_{ab} has been computed by summing or averaging the coherent metrics $g_{ab}^{(i)}$ for the $i = 1, \dots, M$ segments of the coherent searches [77–79, 83, 85]. This averaged metric can be a poor approximation, and recent work has investigated its accuracy and empirical ways to extend the range of validity [91].

This work suggests a possible improvement. Instead of estimating the semi-coherent mismatch with an averaged metric

$$m = \bar{g}_{ab} d\lambda^a d\lambda^b = \frac{1}{M} \sum_{i=1}^M g_{ab}^{(i)} d\lambda^a d\lambda^b, \quad (7.3)$$

it might be more accurate to instead compute the semi-coherent mismatch in the spherical approximation:

$$m = \frac{1}{M} \sum_{i=1}^M \sin^2 \sqrt{g_{ab}^{(i)} d\lambda^a d\lambda^b}. \quad (7.4)$$

Because the sin-squared of the average is not the average of the sin-squared, Eqs. 7.3 and 7.4 could differ substantially, particularly if the quadratic approximation to the metric significantly overestimates the mismatch in one or more of the coherent segments.

VIII. CONVENTIONS FOR OVERLAP AND MISMATCH

In much of the CBC literature the mismatch is defined as

$$m(\lambda, \lambda') = 1 - o(\lambda, \lambda'). \quad (8.1)$$

This SNR fractional mismatch should be contrasted with the SNR² fractional mismatch defined in Eq. (2.1). With this definition of the mismatch, the same considerations as above give the spherical approximation as

$$\begin{aligned} m &= 1 - \cos \sqrt{g_{ab} d\lambda^a d\lambda^b} \\ &= 2 \sin^2 \frac{1}{2} \sqrt{g_{ab} d\lambda^a d\lambda^b}. \end{aligned}$$

This should be contrasted with the spherical approximation given in Eq. (4.2).

IX. CONCLUSION

For three typical examples, we have shown that replacing the conventional metric mismatch $g_{ab} d\lambda^a d\lambda^b$ with $\sin^2 \sqrt{g_{ab} d\lambda^a d\lambda^b}$ gives a better approximation to the true template mismatch. We have argued that this is to be expected in the generic case, and suggested that averaging the spherical approximation might provide a more accurate way to compute the mismatch in semi-coherent searches.

I thank Curt Cutler, Maria Alessandra Papa and Reinhard Prix for encouragement and helpful comments, and Ben Owen and B.S. Sathyaprakash for teaching me about matched filtering and metrics.

-
- [1] B. F. Schutz, *Classical and Quantum Gravity* **6**, 1761 (1989).
- [2] *NATO Advanced Science Institutes (ASI) Series C*, Vol. 253 (1989).
- [3] B. S. Sathyaprakash and S. V. Dhurandhar, *Phys. Rev. D* **44**, 3819 (1991).
- [4] B. F. Schutz, in *The Detection of Gravitational Waves*, edited by D. G. Blair (1991) p. 406.
- [5] L. S. Finn and D. F. Chernoff, *Phys. Rev. D* **47**, 2198 (1993), arXiv:gr-qc/9301003 [gr-qc].
- [6] C. Cutler, T. A. Apostolatos, L. Bildsten, L. S. Finn, E. E. Flanagan, D. Kennefick, D. M. Markovic, A. Ori, E. Poisson, G. J. Sussman, and K. S. Thorne, *Phys. Rev. Lett.* **70**, 2984 (1993), arXiv:astro-ph/9208005 [astro-ph].
- [7] B. S. Sathyaprakash, *Phys. Rev. D* **50**, R7111 (1994), arXiv:gr-qc/9411043 [gr-qc].
- [8] C. Cutler and E. E. Flanagan, *Phys. Rev. D* **49**, 2658 (1994), arXiv:gr-qc/9402014 [gr-qc].
- [9] T. A. Apostolatos, C. Cutler, G. J. Sussman, and K. S. Thorne, *Phys. Rev. D* **49**, 6274 (1994).
- [10] T. A. Apostolatos, *Phys. Rev. D* **52**, 605 (1995).
- [11] S. V. Dhurandhar and B. S. Sathyaprakash, *Phys. Rev. D* **49**, 1707 (1994).
- [12] S. V. Dhurandhar and B. F. Schutz, *Phys. Rev. D* **50**, 2390 (1994).
- [13] R. Balasubramanian and S. V. Dhurandhar, *Phys. Rev. D* **50**, 6080 (1994), arXiv:gr-qc/9404009 [gr-qc].
- [14] R. Balasubramanian, B. S. Sathyaprakash, and S. V. Dhurandhar, *Phys. Rev. D* **53**, 3033 (1996), arXiv:gr-qc/9508011 [gr-qc].
- [15] R. Balasubramanian, B. S. Sathyaprakash, and S. V. Dhurandhar, *Phys. Rev. D* **54**, 1860 (1996).
- [16] B. J. Owen and B. S. Sathyaprakash, *Phys. Rev. D* **60**, 022002 (1999), arXiv:gr-qc/9808076 [gr-qc].
- [17] In many cases of interest a quantity corresponding to SNR is analytically maximized over some intrinsic phase parameters. This results in a “squared-SNR” detection statistic which is quadratic in the data. The mismatch we define then corresponds to the fractional loss of expected squared SNR in the strong signal limit.
- [18] L. A. Wainstein and V. D. Zubakov, *Extraction of Signals from Noise* (Dover, 1970).
- [19] C. W. Helstrom and F. L. Wilson, *Physics Today* **23**, 73 (1970).
- [20] P. Jaranowski and A. Krolak, *Analysis of Gravitational-Wave Data* (Cambridge University Press, 2009).
- [21] J. Creighton and W. Anderson, *Gravitational-Wave Physics and Astronomy: An Introduction to Theory, Experiment and Data Analysis*. (Wiley, 2011).
- [22] If the signal is narrow-band, then to get the most SNR the instrument output should be filtered so that $n(t)$ only contains the band of interest.
- [23] B. Allen, W. G. Anderson, P. R. Brady, D. A. Brown, and J. D. E. Creighton, *Phys. Rev. D* **85**, 122006 (2012), arXiv:gr-qc/0509116 [gr-qc].
- [24] T. A. Apostolatos, *Phys. Rev. D* **54**, 2421 (1996).
- [25] T. Cokelaer, S. Babak, and B. S. Sathyaprakash, *Classical and Quantum Gravity* **21**, S1635 (2004).
- [26] S. Babak, R. Balasubramanian, D. Churches, T. Cokelaer, and B. S. Sathyaprakash, *Classical and Quantum Gravity* **23**, 5477 (2006), arXiv:gr-qc/0604037 [gr-qc].
- [27] I. W. Harry, B. Allen, and B. S. Sathyaprakash, *Phys. Rev. D* **80**, 104014 (2009), arXiv:0908.2090 [gr-qc].
- [28] C. Messenger, R. Prix, and M. A. Papa, *Phys. Rev. D* **79**, 104017 (2009), arXiv:0809.5223 [gr-qc].
- [29] G. M. Manca and M. Vallisneri, *Phys. Rev. D* **81**, 024004 (2010), arXiv:0909.0563 [gr-qc].
- [30] D. A. Brown, P. Kumar, and A. H. Nitz, *Phys. Rev. D* **87**, 082004 (2013), arXiv:1211.6184 [gr-qc].
- [31] H. Fehrmann and H. J. Pletsch, *Phys. Rev. D* **90**, 124049 (2014), arXiv:1411.3899 [astro-ph.IM].
- [32] P. Kumar, I. MacDonald, D. A. Brown, H. P. Pfeiffer, K. Cannon, M. Boyle, L. E. Kidder, A. H. Mroué, M. A. Scheel, B. Szilágyi, and A. Zenginoglu, *Phys. Rev. D* **89**, 042002 (2014), arXiv:1310.7949 [gr-qc].
- [33] S. Roy, A. S. Sengupta, and N. Thakor, *Phys. Rev. D* **95**, 104045 (2017), arXiv:1702.06771 [gr-qc].
- [34] Some parameters are NOT included in λ . For example the

- (normalized) templates are independent of the distance to the source. For search techniques based on fast Fourier transforms (FFTs) the coalescence time or signal phase might be left out because they are automatically searched over.
- [35] P. R. Brady, T. Creighton, C. Cutler, and B. F. Schutz, *Phys. Rev. D* **57**, 2101 (1998), arXiv:gr-qc/9702050 [gr-qc].
- [36] P. R. Brady and T. Creighton, *Phys. Rev. D* **61**, 082001 (2000), arXiv:gr-qc/9812014 [gr-qc].
- [37] P. Jaranowski, A. Królak, and B. F. Schutz, *Phys. Rev. D* **58**, 063001 (1998), arXiv:gr-qc/9804014 [gr-qc].
- [38] A. Píarski, P. Jaranowski, and M. Pietka, *Phys. Rev. D* **83**, 043001 (2011), arXiv:1010.2879 [gr-qc].
- [39] K. Wette, S. Walsh, R. Prix, and M. A. Papa, *Phys. Rev. D* **97**, 123016 (2018), arXiv:1804.03392 [astro-ph.IM].
- [40] B. J. Owen, *Phys. Rev. D* **53**, 6749 (1996), arXiv:gr-qc/9511032 [gr-qc].
- [41] Y. Chen, *Topics of LIGO physics: Quantum noise in advanced interferometers and template banks for compact binary inspirals*, Ph.D. thesis, CALIFORNIA INSTITUTE OF TECHNOLOGY (2003).
- [42] R. P. Croce, T. Demma, M. Longo, S. Marano, V. Matta, V. Pierro, and I. M. Pinto, *Phys. Rev. D* **70**, 122001 (2004), arXiv:gr-qc/0405023 [gr-qc].
- [43] S. K. Sahay, *International Journal of Modern Physics D* **15**, 225 (2006), arXiv:astro-ph/0603749 [astro-ph].
- [44] Y. Pan, *Topics of LIGO physics: Template banks for the inspiral of precessing, compact binaries, and design of the signal-recycling cavity for advanced LIGO*, Ph.D. thesis, California Institute of Technology (2006).
- [45] T. Cokelaer, *Classical and Quantum Gravity* **24**, 6227 (2007), arXiv:0709.1050 [gr-qc].
- [46] R. Prix, *Classical and Quantum Gravity* **24**, S481 (2007), arXiv:0707.0428 [gr-qc].
- [47] T. Cokelaer, *Phys. Rev. D* **76**, 102004 (2007), arXiv:0706.4437 [gr-qc].
- [48] J. T. Whelan, R. Prix, and D. Khurana, *Classical and Quantum Gravity* **25**, 184029 (2008), arXiv:0805.1972 [gr-qc].
- [49] S. Babak, *Classical and Quantum Gravity* **25**, 195011 (2008), arXiv:0801.4070 [gr-qc].
- [50] P. Ajith, S. Babak, Y. Chen, M. Hewitson, B. Krishnan, A. M. Sintes, J. T. Whelan, B. Brügmann, P. Diener, N. Dorband, J. Gonzalez, M. Hannam, S. Husa, D. Pollney, L. Rezzolla, L. Santamaría, U. Sperhake, and J. Thornburg, *Phys. Rev. D* **77**, 104017 (2008), arXiv:0710.2335 [gr-qc].
- [51] T. Cokelaer and D. Pathak, *Classical and Quantum Gravity* **26**, 045013 (2009), arXiv:0903.4791 [gr-qc].
- [52] P. Ajith, S. Babak, Y. Chen, M. Hewitson, B. Krishnan, A. M. Sintes, J. T. Whelan, B. Brügmann, P. Diener, N. Dorband, J. Gonzalez, M. Hannam, S. Husa, D. Pollney, L. Rezzolla, L. Santamaría, U. Sperhake, and J. Thornburg, *Phys. Rev. D* **79**, 129901 (2009).
- [53] C. van den Broeck, R. A. Brown, T. Cokelaer, I. Harry, G. Jones, B. S. Sathyaprakash, H. Tagoshi, and H. Takahashi, *Phys. Rev. D* **80**, 024009 (2009), arXiv:0904.1715 [gr-qc].
- [54] J. T. Whelan, R. Prix, and D. Khurana, *Classical and Quantum Gravity* **27**, 055010 (2010), arXiv:0908.3766 [gr-qc].
- [55] D. Keppel, *Phys. Rev. D* **87**, 124003 (2013), arXiv:1303.2005 [physics.data-an].
- [56] P. Ajith, N. Fotopoulos, S. Privitera, A. Neunzert, N. Mazumder, and A. J. Weinstein, *Phys. Rev. D* **89**, 084041 (2014), arXiv:1210.6666 [gr-qc].
- [57] A. Píarski and P. Jaranowski, *Classical and Quantum Gravity* **32**, 145014 (2015), arXiv:1302.0509 [gr-qc].
- [58] A. J. K. Chua and J. R. Gair, *Phys. Rev. D* **93**, 122001 (2016).
- [59] N. Indik, K. Haris, T. Dal Canton, H. Fehrmann, B. Krishnan, A. Lundgren, A. B. Nielsen, and A. Pai, *Phys. Rev. D* **95**, 064056 (2017), arXiv:1612.05173 [gr-qc].
- [60] T. Dal Canton and I. W. Harry, arXiv e-prints , arXiv:1705.01845 (2017), arXiv:1705.01845 [gr-qc].
- [61] S. Roy, A. S. Sengupta, and P. Ajith, arXiv e-prints , arXiv:1711.08743 (2017), arXiv:1711.08743 [gr-qc].
- [62] D. Mukherjee, S. Caudill, R. Magee, C. Messick, S. Privitera, S. Sachdev, K. Blackburn, P. Brady, P. Brockill, K. Cannon, S. J. Chamberlin, D. Chatterjee, J. D. E. Creighton, H. Fong, P. Godwin, C. Hanna, S. Kapadia, R. N. Lang, T. G. F. Li, R. K. L. Lo, D. Meacher, A. Pace, L. Sadeghian, L. Tsukada, L. Wade, M. Wade, A. Weinstein, and L. Xiao, arXiv e-prints , arXiv:1812.05121 (2018), arXiv:1812.05121 [astro-ph.IM].
- [63] S. Roy, A. Sankar Sengupta, and P. Ajith, in *42nd COSPAR Scientific Assembly*, Vol. 42 (2018) pp. E1.15–36–18.
- [64] S. Roy, A. S. Sengupta, and P. Ajith, *Phys. Rev. D* **99**, 024048 (2019).
- [65] J. Roulet, L. Dai, T. Venumadhav, B. Zackay, and M. Zaldarriaga, arXiv e-prints , arXiv:1904.01683 (2019), arXiv:1904.01683 [astro-ph.IM].
- [66] Typically waveforms can have either sign, so one can constrain this overlap to the closed interval $[0, 1]$.
- [67] Suppose that the mismatch is minimized with respect to template parameters α, \dots, β , and that the templates are a continuous function of these parameters. Then the results given here still hold, because at the extrema one may express each of these parameters as a function of the remaining free parameters, i.e. one has $\alpha(\lambda, \lambda'), \dots, \beta(\lambda, \lambda')$.
- [68] This is very similar to the way that a normalized wavefunction in quantum mechanics is expressed as an infinite sum of coefficients multiplying basis vectors.
- [69] R. Prix, *Phys. Rev. D* **75**, 023004 (2007), arXiv:gr-qc/0606088 [gr-qc].
- [70] R. Prix, *Phys. Rev. D* **75**, 069901 (2007).
- [71] About two decades ago, Benjamin Owen pointed this out to me, and told me that it was an effect arising from “projection onto the sphere”. He was right!
- [72] Note that the exact behavior of the mismatch as a function of the parameter coordinate separation depends upon the parameterization of the waveforms. Any non-linear transformation of the parameter will change this behavior, but a “generic” choice of parameterization will not. A generic parameterization is one for which the angle θ sweeps steadily along the sphere.
- [73] S. D. Mohanty and S. V. Dhurandhar, *Phys. Rev. D* **54**, 7108 (1996).
- [74] S. D. Mohanty, *Phys. Rev. D* **57**, 630 (1998), arXiv:gr-qc/9703081 [gr-qc].
- [75] B. Allen, J. K. Blackburn, P. R. Brady, J. D. Creighton, T. Creighton, S. Droz, A. D. Gillespie, S. A. Hughes, S. Kawamura, T. T. Lyons, J. E. Mason, B. J. Owen, F. J. Raab, M. W. Regehr, B. S. Sathyaprakash, R. L. Savage, S. Whitcomb, and A. G. Wiseman, *Phys. Rev.*

- Lett. **83**, 1498 (1999), arXiv:gr-qc/9903108 [gr-qc].
- [76] D. A. Brown, J. Crowder, C. Cutler, I. Mandel, and M. Vallisneri, *Classical and Quantum Gravity* **24**, S595 (2007), arXiv:0704.2447 [gr-qc].
- [77] K. Wette, *Phys. Rev. D* **92**, 082003 (2015), arXiv:1508.02372 [gr-qc].
- [78] H. J. Pletsch and B. Allen, *Phys. Rev. Lett.* **103**, 181102 (2009), arXiv:0906.0023 [gr-qc].
- [79] H. J. Pletsch, *Phys. Rev. D* **82**, 042002 (2010), arXiv:1005.0395 [gr-qc].
- [80] H. J. Pletsch, *Phys. Rev. D* **83**, 122003 (2011), arXiv:1101.5396 [gr-qc].
- [81] H. J. Pletsch, L. Guillemot, B. Allen, M. Kramer, C. Aulbert, H. Fehrmann, P. S. Ray, E. D. Barr, A. Belfiore, F. Camilo, P. A. Caraveo, Ö. Çelik, D. J. Champion, M. Dormody, R. P. Eatough, E. C. Ferrara, P. C. C. Freire, J. W. T. Hessels, M. Keith, M. Kerr, A. de Luca, A. G. Lyne, M. Marelli, M. A. McLaughlin, D. Parent, S. M. Ransom, M. Razzano, W. Reich, P. M. Saz Parkinson, B. W. Stappers, and M. T. Wolff, *Astrophys. J.* **744**, 105 (2012), arXiv:1111.0523 [astro-ph.HE].
- [82] M. Shaltev and R. Prix, *Phys. Rev. D* **87**, 084057 (2013), arXiv:1303.2471 [gr-qc].
- [83] K. Wette and R. Prix, *Phys. Rev. D* **88**, 123005 (2013), arXiv:1310.5587 [gr-qc].
- [84] H. J. Pletsch and C. J. Clark, *Astrophys. J.* **795**, 75 (2014), arXiv:1408.6962 [astro-ph.HE].
- [85] P. Leaci and R. Prix, *Phys. Rev. D* **91**, 102003 (2015), arXiv:1502.00914 [gr-qc].
- [86] B. P. Abbott *et al.* (LIGO/Virgo Scientific Collaboration), *Phys. Rev. D* **96**, 062002 (2017), arXiv:1707.02667 [gr-qc].
- [87] B. P. Abbott *et al.* (LIGO/Virgo Scientific Collaboration), *Phys. Rev. D* **96**, 122004 (2017), arXiv:1707.02669 [gr-qc].
- [88] C. J. Clark, J. Wu, H. J. Pletsch, L. Guillemot, B. Allen, C. Aulbert, C. Beer, O. Bock, A. Cuéllar, H. B. Eggenstein, H. Fehrmann, M. Kramer, B. Machenschalk, and L. Nieder, *Astrophys. J.* **834**, 106 (2017), arXiv:1611.01015 [astro-ph.HE].
- [89] C. Dreissigacker, R. Prix, and K. Wette, *Phys. Rev. D* **98**, 084058 (2018), arXiv:1808.02459 [gr-qc].
- [90] L. Nieder, C. J. Clark, and H. J. Pletsch, in *Pulsar Astrophysics the Next Fifty Years*, IAU Symposium, Vol. 337, edited by P. Weltevrede, B. B. P. Perera, L. L. Preston, and S. Sanidas (2018) pp. 382–383.
- [91] K. Wette, *Phys. Rev. D* **94**, 122002 (2016), arXiv:1607.00241 [gr-qc].